Unraveling the intricacies of surface salt formation on Mg(0001): Implications for chloride-ion batteries

Kanchan Sarkar,[1] Darius Hübner,[1] Daniel Stottmeister,[1] and Axel Groß[1,2]
[1]*Institute of Theoretical Chemistry, Ulm University, 89069 Ulm, Germany*
[2]*Helmholtz Institute Ulm, Electrochemical Energy Storage, 89081 Ulm, Germany*

(Received 4 October 2023; accepted 14 December 2023; published 5 January 2024)

We present a density functional theory study of the initial steps of chlorine deposition on the Mg(0001) surface. Such processes occur in chloride-ion batteries in which lithium and magnesium are used as anode materials. In addition, it is also of fundamental interest, as halide adsorption on metal electrodes is an important process in interfacial electrochemistry. We discuss the adsorption properties and determine the stable adsorption structures, both with respect to the free chlorine molecule but also as a function of the electrode potential. We find indications of the immediate formation of the $MgCl_2$ surface salt structure upon exposure of Cl to a Mg surface. These findings are discussed with respect to the conversion of the Mg anode to a $MgCl_2$ configuration which provides the thermodynamical driving force for the discharge of a Cl-ion battery.

DOI: 10.1103/PhysRevMaterials.8.015401

I. INTRODUCTION

The interaction of halides with metal anodes is of general interest in electrochemistry, as halides are typical anions present in electrolytes [1–3]. Understanding the interaction between adsorbates and metal surfaces is essential for designing efficient electrode materials for energy storage and conversion applications [4]. Recently, the interaction of chloride with lithium and magnesium electrodes has become of interest in the context of chloride-ion batteries [5–7] in which lithium and magnesium can be used as the anode material [8]. Batteries based on anions such as chloride represent an alternative to the widely used Li-ion batteries as they are typically based on more abundant materials and also exhibit theoretical energy densities which can be higher than those of current lithium-ion batteries [9,10]. Thus they contribute to more sustainable and environmentally friendly energy storage technologies.

Yet, the interaction of halides with metal surfaces is also interesting from a surface science point of view. It has been known for a long time that the adsorption of halogen atoms on metal surfaces can lead to an anomalous decrease in the work function [11–14]. Typically, one would expect that the adsorption of negatively charged species such as anions on a surface would lead to a dipole moment at the surface that would increase the work function of the metal surface. Results of first-principles electronic structure calculations using density functional theory (DFT) have demonstrated that this anomalous behavior can be attributed to a strong polarization of the halogen atoms upon adsorption [15–17].

To the best of our knowledge, the adsorption of chlorine on magnesium has not been intensively studied yet from a computational point of view. The existing studies were motivated by the fact that chlorine adsorption could lead to the corrosion of Mg metals [18–20]. These computational studies found that Cl preferentially adsorbs in the threefold hollow positions on Mg(0001) associated with a slight increase in the work function. Upon the operation of Cl-ion batteries, the metal anode will be converted to a chloride salt which provides the thermodynamical driving force for the discharge of a Cl-ion battery. The energy gain upon this conversion does in fact represent the driving force in the Cl-ion battery operation [5,6]. This means that the adsorption of chlorine on the metal anode does only correspond to the first step in the anode conversion upon discharge. Still, it is interesting from a fundamental as well as from an applied point of view how the overall conversion of the metal anode on Cl-ion batteries from a bulk metal to a chloride salt proceeds.

Expanding our inquiry to surface films on metal electrodes reveals their pivotal yet largely unexplored role across various applications, encompassing batteries, corrosion, and electrochemical processes. While our paper sheds light on chlorine adsorption on the Mg(0001) surface, providing insights for metal-ion battery technologies, it also confronts broader challenges inherent in modeling metal-surface interfaces. Specifically, interfaces between metals and transition metal oxides, such as the austenitic "steel metal"/Fe_2O_3 interface, have remained underexplored within the realm of DFT methods. Unlike the well-established studies on the Al/Al_2O_3 interface, where initial modeling lacked major reconstruction [21], recent advancements underscore the imperative for precise characterization of interfacial structures. The significant impact of the Al/Al_2O_3 interface on contact potential, electronic properties, and electrochemical behaviors pertaining to aluminum corrosion accentuates the critical need for further research in this domain [22,23].

Our paper also finds resonance in corrosion science [24] studies and electrochemistry [25]. The characterization of salt films on metallic surfaces has revealed porous structures with coprecipitated salts and self-regulating mechanisms [24]. Leveraging advanced techniques such as cryo-based focused ion beam/scanning electron microscopy, these studies

showcase intricate details of salt film structures, revealing interconnected channels for ionic transport [24]. The understanding of chloride's role in corrosion, including its adsorption energies and environmental conditions, as presented in [25], enriches the fundamental insights into the interactions of chloride with metallic surfaces. While our primary focus is on chloride adsorption on Mg(0001) for Cl-ion batteries, drawing parallels with corrosion-related investigations provides additional motivation for exploring the thermodynamically stable chlorine adsorbate structures on Mg(0001) substrates in various electrochemical environments. This sheds light on the potential conversion of Mg anodes in chloride-ion batteries and unveils possibilities for designing corrosion-resistant alloys.

Moreover, scant attention has been dedicated in the literature to the thickness of well-defined $MgCl_2$ layers on Mg metal in chloride-containing electrolytes. Existing studies often focus on passivation films composed of mixed $MgCl_2$ and other magnesium chloride-based compounds. Leong *et al.* [26] present a reversible Mg metal battery using a $MgCl_2$ water-in-salt electrolyte, transforming the passivation film into a conductive Mg–MgO interphase. In another investigation of $MgTFSI_2/MgCl_2$ electrolyte solutions in dimethoxyethane, promising for secondary Mg batteries, structural analysis identifies complex solvated ions formed in the solutions [27]. While advancements are made in understanding $MgCl_2$-containing electrolytes, explicit discussions on $MgCl_2$ layer thickness on Mg metal from experimental Mg battery literature are limited and merit further exploration.

Continuing our inquiry into metal-surface interactions, it is well established that metals can form so-called surface oxides, i.e., thin adsorbed films with an oxidelike structure, upon the exposure of metals to an oxygen atmosphere as a function of the oxygen concentration [28,29]. Hence the question arises whether metal surfaces upon the exposure to halogen species might form equivalent structure corresponding to a *surface salt*, i.e., thin films with metal-halide-like structures. In fact, the existence of Pb-NO_3 surface salts has been predicted by first-principles calculations for Pb(111) electrodes in the presence of a nitrate electrolyte [30,31]. These surface salts have been suggested to be instrumental in the functioning of atomic-scale transistors [31–33].

In the computational study reported in this paper, we will consider the adsorption of chlorine on the most stable surface termination of magnesium, Mg(0001) [34], for a range of different coverages by means of density functional theory calculations. Using grand-canonical concepts [35–38], we will determine the thermodynamically stable chlorine surface structures on Mg(0001) as a function of electrochemical control parameters. Thus we will test whether surface salt structures might be a stable intermediate in the conversion of a Mg anode to $MgCl_2$ upon discharge of a Mg-ion battery.

II. COMPUTATIONAL DETAILS

We have used the Vienna Ab Initio Simulation Package (VASP) [39,40] to perform periodic DFT calculations which are well suited to tackle basic battery-relevant problems [41]. Exchange-correlation effects have been taken into account within the generalized gradient approximation employing the

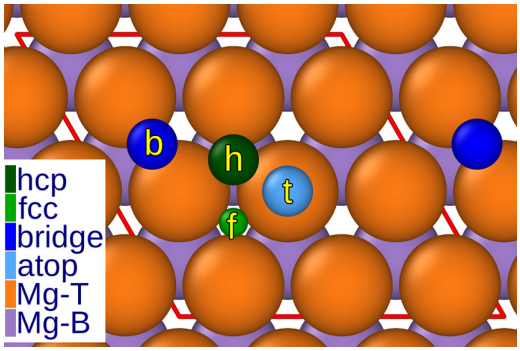

FIG. 1. Different adsorption sites on the Mg (0001) surface, indicating their positions relative to the underlying surface structure. The surface is depicted as a slab, with the top layer represented by Mg-T atoms and the seven bottom layers represented by Mg-B atoms. The adsorption sites, including hcp (hexagonal close packed), fcc (face-centered cubic), bridge, and atop, are indicated by small spheres of different colors.

functional of Perdew, Burke, and Ernzerhof (PBE) [42], as this functional is well suited to reproduce the properties of metals [2,43]. The core electrons are represented by projector augmented wave pseudopotentials [44] as supplied in VASP [45]. An energy cutoff of 810 eV has been chosen in the expansion of the wave functions in plane waves in order to safely ensure convergence of the results. Likewise, a $16 \times 16 \times 16$ Monkhorst-Pack k-point grid has been used for the bulk metal calculations and $5 \times 5 \times 1$ k points were used for the eight-layer slab calculations with 3×3 surface unit cells yielding converged results for the integration over the first Brillouin zone. The slabs were separated by 15 Å of vacuum. The electronic tolerance at each ionic step has been chosen to be 10^{-7} eV based on a Gaussian smearing of 0.02 eV width.

Magnesium crystallizes in the hcp structure. The computed equilibrium lattice parameters for bulk hcp-Mg ($a = 3.195$ Å and $c/a = 1.627$) agree well with experimental values of 3.21 Å and 1.62. Likewise, the calculated cohesive energy of -1.52 eV/atom compares nicely with the experimental results (-1.51 eV/atom) [46–48]. Mg(0001) corresponds to a hexagonal close-packed surface. The layers of Mg(0001) are relaxed until the force on every atom is smaller than 0.01 eV/Å to secure convergence. Surface energetics and electronic structures have been explored first using 0.1 eV Methfessel-Paxton smearing followed by a final energy extrapolation to zero broadening.

The high symmetry sites of Mg (0001) correspond to atop, hcp, fcc, and bridge positions (see Fig. 1). As described in detail below, the hollow site (hcp or fcc) is affirmed to be the favored adsorption site over the bridge and on-top positions. The relative stabilities go on as f (fcc) $\sim h$ (hcp) $> t$ (top) $\gg b$ (bridge). On-surface atop and bridge positions are metastable and unstable, respectively. Therefore, we focus on fcc, hcp, or both these adsorption locales alongside top positions with coverages between 0.11 and 2.44 ML. Also, we perform adsorption calculations over one face by comparing computational outcomes for both the single- and double-faced metal slabs.

The adsorption energies E_{ads} per adsorbate of N_{ads} adsorbates within a given unit cell have been calculated

according to

$$E_{\text{ads}} = \frac{1}{N_{\text{ads}}}[E_{\text{tot}} - (E_{\text{surf}} + N_{\text{ads}}E_{\text{a}})], \tag{1}$$

where E_{surf} and E_{a} are the total energies of the clean surface and the adsorbate in its most stable structure, respectively, and E_{tot} is the total energy of the adsorption system. The most stable form of chlorine is the Cl_2 molecule in the gas phase, so that E_{a} corresponds to half of the binding energy of the Cl_2 molecule. Note furthermore that with the binding energy of stable adsorbates we denote the absolute value of the adsorption energy, $E_b = |E_{\text{ads}}|$.

Note that thermodynamically the stable adsorbate structures are not determined by the adsorption energy per adsorbate, but rather by the adsorption energy per surface area. Furthermore, under equilibrium conditions the energy of the adsorbates is given by the adequate chemical or electrochemical potential. Thus the central quantity is the free surface energy of adsorption [37]:

$$\begin{aligned}\Delta\gamma(T, p) &= \frac{\Delta G_{\text{ads}}(T, p)}{A_s} \\ &= \frac{1}{A_s}[G_{\text{ads}}(T, p, N_{\text{ads}}) - G_{\text{ads}}(T, p, 0) \\ &\quad - N_{\text{ads}}\,\mu_{\text{ads}}(T, p)].\end{aligned} \tag{2}$$

In electrochemical systems, the electrochemical potential instead of the chemical potential enters the determination of the surface energy of adsorption. In order to obtain convenient expressions for the electrochemical potential, we use the concept of the computational hydrogen electrode (CHE) [36] which can also be applied to the adsorption of halogen atoms such as chlorine using the redox couple $\frac{1}{2}\,Cl_2 + e^- \rightleftarrows Cl^-$ [49,50] yielding an electrochemical potential of

$$\begin{aligned}\tilde{\mu}(Cl^-(aq)) - \mu(e^-) = \tfrac{1}{2}\mu(Cl_2(g)) + e\big(U_{\text{SHE}} - U^0\big) \\ + k_{\text{B}}T\ln a_{Cl^-}.\end{aligned} \tag{3}$$

Here, $U^0 = 1.36$ is the reduction potential of the chloride vs U_{SHE} [49,50] and a_{Cl^-} is its activity coefficient. Finally, we replace the free energy G_{ads} appearing in Eq. (2) by the total energy E_{ads} per adsorbate which is often done in applications of the CHE concept and which typically still yields satisfactory results for the adsorption of strongly bound small adsorbates such as hydrogen and chlorine [38]. Thus we obtain the following expression of the free surface energy of adsorption as a function of the electrode potential:

$$\Delta\gamma(U_{\text{SHE}}) = \frac{N_{\text{ads}}}{A_s}\big(E_{\text{ads}} - e(U_{\text{SHE}} - U^0)\big), \tag{4}$$

where we assume standard conditions, which means that the activity of the halides a_{A^-} is unity. For other concentrations of the halides, the electrode potential needs to be shifted by $k_{\text{B}}T\ln a_{A^-}$ which corresponds to 59 meV for a change of the activity by one order of magnitude at room temperature.

III. RESULTS AND DISCUSSION

A. Interlayer spacing on the Mg(0001) surface

The behavior of the Mg(0001) surface deviates significantly from conventional metal surfaces, as evidenced by an unconventional expansion in the first interlayer spacing compared to its bulk structure. Typically, the topmost atoms on a metal surface layer form stronger bonds with the underlying layer, leading to a contraction in the interlayer spacing [51,52]. However, both computational simulations and experimental studies provide compelling evidence supporting an approximate expansion of 1.95% in the first interlayer spacing for the Mg(0001) surface [53–55].

While the behavior of the first interlayer spacing on the Mg(0001) surface has received considerable attention and is thus well documented [53–55], the second interlayer spacing has sparked debate in the literature. Notably, experimental findings by Sprunger *et al.* [54] and theoretical estimates [53] (and references therein) indicate an expansion of approximately 0.8%. In contrast, our calculations, complemented by atomic structure analysis employing low-energy electron diffraction [55] intensity measurements, reveal a slight reduction of about −0.03%. Although this discrepancy may seem subtle, it underscores the intricate nature of interlayer interactions on the Mg(0001) surface and emphasizes the significance of precision in future investigations. We ensured accuracy and precision in our calculations by employing enhanced computational settings, as outlined in the computational methods section. Additionally, we expanded the system to include eight layers, as a well-converged interlayer relaxation necessitates at least seven layers for the hcp Mg(0001) surface, analogous to surface energy and work function studies [53]. Regarding the subsequent interlayer spacings, we observed the following changes with respect to the ideal spacing: −0.16 (expt. 0.4 ± 0.4 [54] and 0.0% [55]), −0.1, −0.16, −0.03, and 1.95%.

B. Cl adatom adsorption preferences and energetics on the hcp Mg(0001) surface

As far as the adsorption behavior on hcp metal surfaces is concerned, computational studies consistently demonstrate that typically the most stable adsorption configurations are found at the hollow (hcp and fcc) sites and the bridge site [51,52], as evidenced by the calculated binding energy (E_b). These sites offer favorable interactions due to the proximity and coordination of the adsorbate with the surface atoms, resulting in a stronger binding. In contrast, the atop site, lacking neighboring metal substrate atoms, exhibits weaker bonding interactions.

For the specific case of Cl adsorption on Mg(0001), we examined the optimal adsorption position for a single Cl adatom within a 3 × 3 unit cell. Note that adsorption of Cl on the Mg(0001) surface predominantly occurs on the surface rather than filling the subsurface tetra or octasites [56]. Consistent with the observed trend, we found that the hcp site exhibits the most favorable adsorption with an adsorption energy of −2.587 eV, closely followed by the fcc site with an adsorption energy of −2.581 eV. These results indicate a preference for high-coordinated adsorption sites on Mg(0001). Notably, the singly coordinated top site emerges as the next most favorable adsorption site with an energy of −2.308 eV, while the doubly coordinated bridge site corresponds to an unstable local maximum. Cl binding to Mg(0001) is thus by about 0.6 eV stronger than to Cu(111), but considerably weaker by about

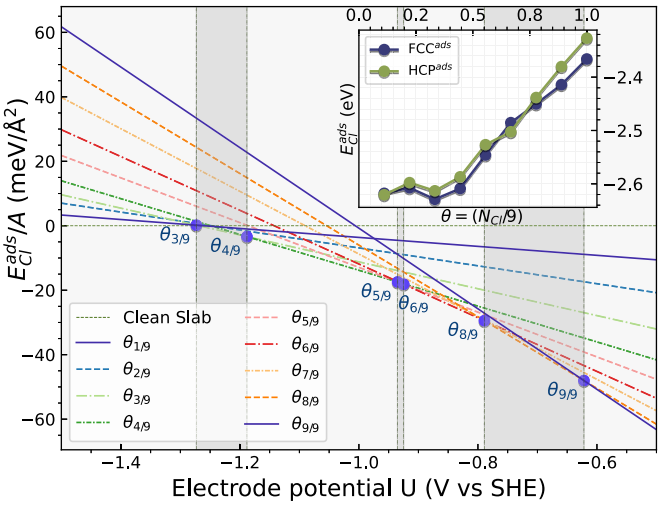

FIG. 2. Free surface energies of adsorption for chlorine adsorption structures as a function of the electrode potential for surface coverages between 1/9 and 1. The stable structures are given by lowest surface energies as a function of the electrode potential. The inset shows the adsorption energy per Cl atom as a function of coverage for adsorption at the fcc and hcp sites.

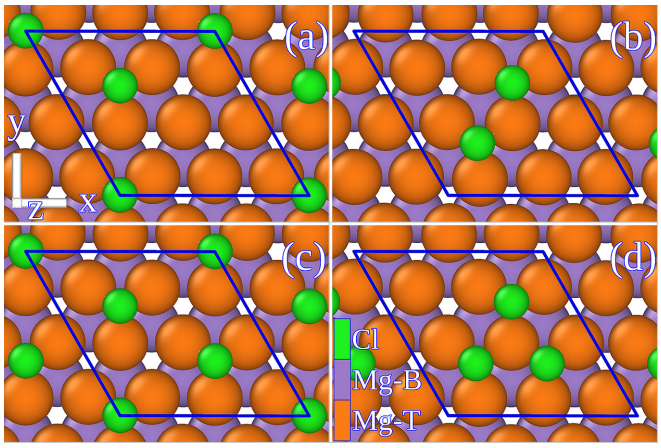

FIG. 3. Structural arrangement of Cl adsorption sites at Cl coverages of 2/9 (a), (b) and 1/3 (c), (d).

1.4 eV than Cl adsorption on Ca(111) and Sr(111) [17,50]. Note furthermore that the energy gain upon Cl adsorption on Mg(0001) is larger than upon $MgCl_2$ formation which is about −1.5 eV per formula unit depending on the particular $MgCl_2$ bulk structure. This means that thermodynamically first the formation of a Cl adsorbate layer on Mg(0001) is stable, and only for higher Cl exposures or higher electrode potentials the formation of $MgCl_2$ bulk becomes feasible.

C. Cl structures on Mg(0001) at higher coverages

In the following, we consider higher chlorine surface coverages within the 3 × 3 surface unit cell. Our primary focus remains on the hcp and fcc positions for Cl adsorption on the Mg(0001) surface, given their higher demonstrated adsorption stability. With respect to the adsorption of chlorine on metal surfaces such as Pt(111) and Cu(111), it is well known that there is a repulsive dipole-dipole interaction between the adsorbates [50] which favors adsorption structures with the largest mutual distance between the adsorbates. The adsorption energies per Cl atom as a function of coverage at the fcc and hcp sites are plotted in the inset of Fig. 2. Except for the coverage 2/3, Cl adsorption at the fcc sites is more stable. Overall the decrease in the binding energies due to the mutual repulsion of the adsorbed Cl atoms is well visible.

Interestingly enough, for a chlorine coverage of 2/9, we find the structure with the two chlorine atoms at adjacent fcc hollow sites with a Cl-Cl distance of 3.5 Å more stable than the structure with a larger mutual distance exceeding 5.2 Å [see Figs. 3(a) and 3(b)]. Furthermore, the binding energy per Cl atom at a coverage of 1/3 in a hexagonally close-packed structure [Fig. 3(d)] is even stronger than at a coverage of 1/9. Such a trend in the Cl adsorption for the 1/3 coverage of halogen atoms has been found before, in particular for Cl/Pt(111) [50]. This has been explained by the fact that this arrangement does not only correspond to a two-dimensional close-packed structure but it is at the same time the arrangement with the largest mutual distances among the adsorbates for a given coverage. Still, it is interesting to note that this behavior is particularly strong for chlorine adsorption on Mg(0001) which might be explained by the larger lattice constant of Mg compared to those of late transition metals which allows the Cl atom to adsorb closer to the surface so that the mutual repulsion is even further reduced.

The free surface energies of adsorption plotted in Fig. 2 yield at the same time a surface phase diagram of the most stable surface adsorbate structures as a function of the electrode potential. At electrode potentials above $U = -1.27$ V, chlorine adsorption sets in with a coverage of 1/3 which will then be replaced at higher electrode potentials by the structure with a coverage of 4/9. A similar behavior as a function of electrode potential has also been obtained for Cl adsorption on Cu(111) and Pt(111) [50].

D. Influence of higher chlorine coverage on the Mg(0001) surface

The adsorption behavior of chlorine on the Mg(0001) surface takes an intriguing turn when additional Cl atoms are introduced after reaching full monolayer coverage ($\Theta = 1.0$). We have been looking for the onset of the formation of a $MgCl_2$ layer on Mg(0001) by using an efficient yet computationally inexpensive optimization algorithm called adaptive random mutation hill climbing (ARMHC) [57–59].

Efforts to engineer minimal energy adsorption structures have predominantly been built around manually crafted initial structural designs, followed by optimization through established techniques rooted in solid-state physics, such as empirical, semiempirical, or DFT calculations. While effective for lower adsorbate coverages, this conventional approach grapples with the challenge of accommodating higher adsorbate loads. However, a promising avenue lies in the application of evolutionary computing (EC) techniques, as demonstrated by Sarkar and Bhattacharyya and their referenced works [57]. In essence, EC approaches encompass a spectrum of optimization strategies inspired by the mechanisms of natural selection and genetic inheritance.

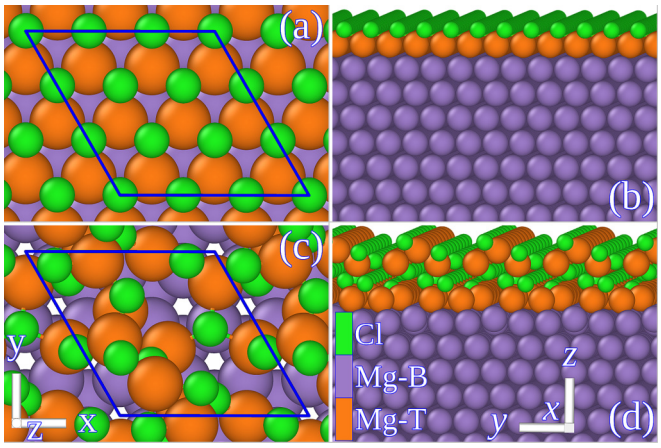

FIG. 4. Top and site views of Cl adsorbate structures at a complete Cl monolayer coverage ($\Theta = 1$) (a), (b) and at a coverage of $\Theta = 10/9$ (c), (d). The surface Mg atoms (Mg-T) are shown in orange, while the lower seven Mg layers (Mg-B) are represented in violet. The Cl atoms are displayed in green. The introduction of an additional Cl atom on the (3×3) surface unit cell disrupts the flat adsorption pattern and leads to a much more open surface structure.

These methods exhibit computational intelligence and inherent adaptability, enabling them to swiftly identify critical regions within the solution space [58].

The employed ARMHC algorithm commences with one initial educated guess and then iteratively refines the positions of the Cl atoms and Mg atoms of the top two surface layers by minimizing the energy determined by single point DFT calculations with low computational setups. For Fig. 4(d), representing a coverage of ten Cl atoms, the initial configuration builds upon previous stoichiometrical structures (nine Cl atoms), with the addition of one extra chlorine atom randomly placed on top. This process is repeated for multiple randomly configured structures, generating a diverse set of low-energy adsorption structures. These initial geometries, tailored to specific adsorbate coverages, are fine tuned using ARMHC, typically converging to the same final minimum energy structure under extensive DFT relaxation studies. The ARMHC algorithm leverages mutation as its sole evolutionary process, with two adjustable parameters – mutation probability and mutation intensity – dynamically fine tuned based on continuous performance evaluation. This strategy involves the random exploration of superior solutions within the vicinity of the current solution by introducing controlled mutations into the adsorption structure. Consequently, ARMHC represents a thoughtfully devised methodology for rapidly generating initial trial solutions in the quest for optimal adsorption structures. For in-depth details, please refer to the code provided in the referenced work [52]. Several plausible initial geometries, tailored to specific adsorbate coverages, have been crafted using the ARMHC algorithm. These geometries are then subjected to rigorous relaxation studies using the DFT code.

By adopting this strategy, we efficiently explored the extensive configuration space and successfully identified stable and energetically favorable arrangements of Cl atoms on the Mg(0001) surface at nominally high coverages, including $\Theta = 10/9, 11/9, 4/3, 13/9,$ and 2.0. This comprehensive investigation allowed us to uncover previously unknown equilibrium structures and gain deeper insights into the adsorption behavior of Cl on the Mg(0001) surface and stability under electrochemical conditions.

In contrast to lower coverages, where simpler adsorption structures tend to dominate, the range of energetically favorable structures becomes notably diverse at $1 < \Theta \leqslant 2$. Accommodating additional Cl atoms on the surface initiates complex adsorption processes, leading to significant reconfiguration of the Mg(0001) surface. Variations in the behavior of surface Mg atoms, involving both elevating and relocating in response to Cl adsorption, result in a multifaceted energy landscape within this coverage range. Numerous local minima with subtle energy differences characterize this landscape, demanding a comprehensive exploration of structural possibilities and their energy landscapes for stability determination. We therefore employed ARMHC algorithms with a variety of wide-ranging initial geometries to fully exploit and explore the complex potential landscapes for each studied coverage in the range of $1 < \Theta \leqslant 2$.

As the chlorine coverage on the Mg(0001) surface approaches and surpasses a monolayer ($\Theta = 1.0$), a notable transition in the surface structure becomes apparent. Figure 4 illustrates this transition through energy minimum structures at nominal Cl coverage of 1 [Figs. 4(a) and 4(b)] and 10/9 [Figs. 4(c) and 4(d)]. In the formation of the $\Theta = 10/9$ structure [Figs. 4(c) or 4(d)], a distinct reconstruction of the Mg surface occurs. Here, Cl atoms, along with the top-layer surface Mg atoms from $\Theta = 1.0$ [Figs. 4(a) or 4(b)], undergo a shift and elevation into the Cl layer and beyond with the introduction of an additional Cl atom. This transition, as the Cl coverage surpasses $\Theta = 1.0$, is characterized by a sudden shift in stability, as evidenced by a significant alteration in the binding energy of 0.23 eV per adsorbed Cl atom. The inset of Fig. 5 illustrates this discontinuity, providing a clear and compelling illustration of the evolving adsorption behavior. It is important to note that the extent and nature of surface reconstructions in the vicinity of the Cl adsorbate layer exhibit a lack of a consistent pattern and instead display significant variation across the $1 < \Theta \leqslant 2$ coverage range. These variations are a consequence of the intricate interplay between Cl-Mg and Cl-Cl interactions, which become increasingly pronounced with the inclusion of extra Cl atoms. Therefore, the intuitive introduction of additional Cl atom(s) to the $\Theta = 10/9$ minimum energy structure does not necessarily lead to a predictable transition to the $\Theta = 11/9$ minimum energy structure or subsequent states. This makes it challenging to foresee specific structural outcomes. However, it is worth mentioning that all the identified energy minimum structures at coverages $1 < \Theta \leqslant 2$ exhibit no Cl-Cl bonding, even when considering a minimum Cl-Cl distance of 3.25 Å for potential bond formation. This observation is in line with experimentally observed trigonal $MgCl_2$ salt structures ($P3\bar{m}1$ and $R\bar{3}m$ [60,61]), which feature a Cl-Cl distance of approximately 3.04 Å. The observations underscore the dynamic nature of the Cl-Mg(0001) system when exposed to higher chloride concentrations, where the interaction between Cl atoms is primarily governed by their interactions with the surface and the surrounding metal atoms, rather than the formation of Cl-Cl bonds.

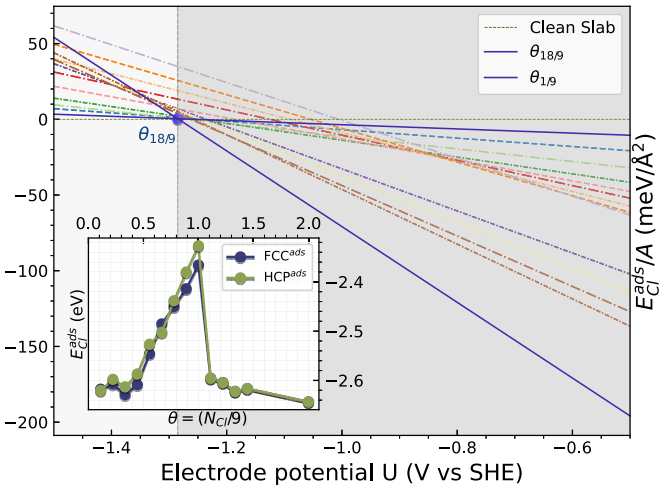

FIG. 5. Free surface energies of adsorption for chlorine adsorption structures as a function of the electrode potential for surface coverages between 1/9 and 2. The stable structures are given by lowest surface energies as a function of the electrode potential. The inset shows the adsorption energy per Cl atom as a function of coverage for adsorption at the fcc and hcp sites on which the free surface energies are based.

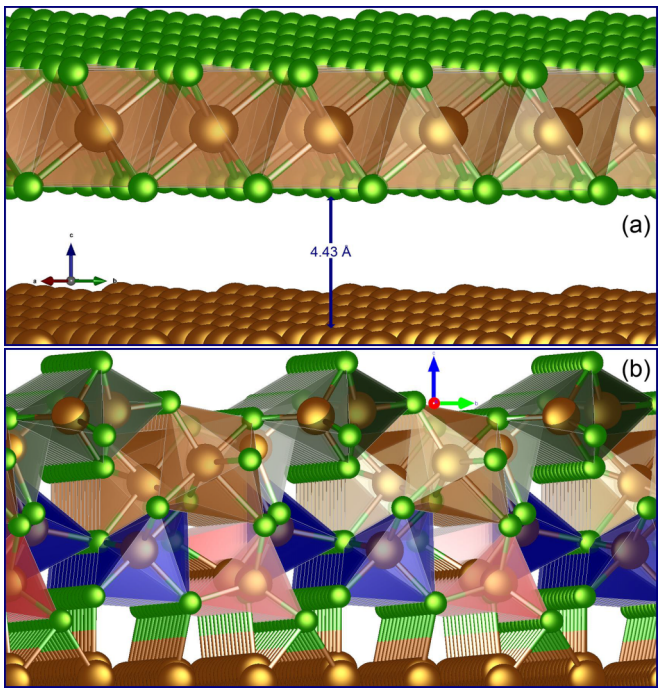

FIG. 6. (a) Illustration of the distinctly separated layered structure of MgCl2 positioned well above the Mg(0001) surface that resulted upon introducing thicker $MgCl_2$ films with a nominally appropriate facet selection in the simulation cell. (b) The most stable Cl adsorbate structure for a nominal Cl coverage of $\Theta_{Cl} = 2$ on Mg(0001) as determined by ARMHC.

The adsorption energies and free surface energies of adsorption as a function of the electrode potential for chlorine coverages $0 < \theta \leqslant 2$ are plotted in Fig. 5. It becomes obvious that $\Theta = 2.0$ is associated with the largest binding energy per chlorine atom among the considered structures (see the inset of Fig. 5). Considering the $\theta = 2$ structure in the plot of the free surface energies of adsorption, it turns out to exhibit a maximum binding energy per Cl atom leading to the lowest onset potential in the phase diagram. In addition, the largest coverage among the considered structures in Fig. 5 leads to a steeper slope of the free surface energies. Thus this structure becomes thermodynamically more stable than all other energetically stable structures with lower coverages. Therefore, upon exposure of the Mg(0001) electrode to chloride at sufficiently high electrode potentials, a saltlike surface structure can be immediately formed as a precursor for the conversion of the Mg electrode to a $MgCl_2$ crystal.

E. Analysis of the formed surface salt structures

In addressing the interface between $MgCl_2$ and Mg(0001), our study reported in this paper encountered a significant challenge stemming from the inherent lack of commensurability between the triangular lattice structure of $MgCl_2$ and the hexagonal close-packed arrangement of Mg(0001). To overcome this, we pursued various strategies, including simulations with enlarged cells and investigations into the impact of thicker $MgCl_2$ films on interface stability within a grand canonical context. The idea of using thicker $MgCl_2$ films as potential buffer layers was considered to enhance the influence of the bulk crystal structure on the outer regions and potentially foster a more stable configuration.

To implement thicker $MgCl_2$ films, we replaced the top layer of Mg atoms with experimentally observed trigonal $MgCl_2$ structures ($P3\bar{m}1$ and $R\bar{3}m$). Despite the initial lattice mismatch of around 14%, computational relaxation and adjustments to the supercell size significantly improved lattice matching. However, achieving commensurability at the interface remained challenging. Even with large simulation cells and careful selection of low-energy facets on a $MgCl_2$ crystal in a grand canonical sense, commensurability was not guaranteed. Adjusting simulation cell parameters often led to nonconvergence or prolonged convergence time towards structures with higher energy. Introducing low-energy $MgCl_2$ crystals resulted in the crystal favoring a high-energy and distinctly separated layered structure of $MgCl_2$, positioned well above the surface [Fig. 6(a)].

Moving forward, we will now present an analysis of the structure of the surface salt formed with a nominal coverage of 2 [see Fig. 6(b)]. In this minimum energy structure [lower by −0.215 eV per adsorbed Cl atom compared to the structure in Fig. 6(a)] found for $\theta = 2$ using ARMHC, intriguing features emerged at the interface between the metal slab and the saltlike structures. At this juncture, where the metal slab meets the saltlike configurations, the Mg atoms exhibited a tricoordinated arrangement, deviating from the typical four to six coordinated Mg atoms found in known $MgCl_2$ salt structures. This tricoordinated arrangement is likely a consequence of the lattice mismatch and symmetrical disparities at the interface between the Mg(0001) surface and the $MgCl_2$ structures, potentially explaining why $MgCl_2$ cannot be deposited on Mg (0001) in a commensurate way. Moving away from the immediate interface along the z axis, coordination environments reminiscent of reported salt structures were observed,

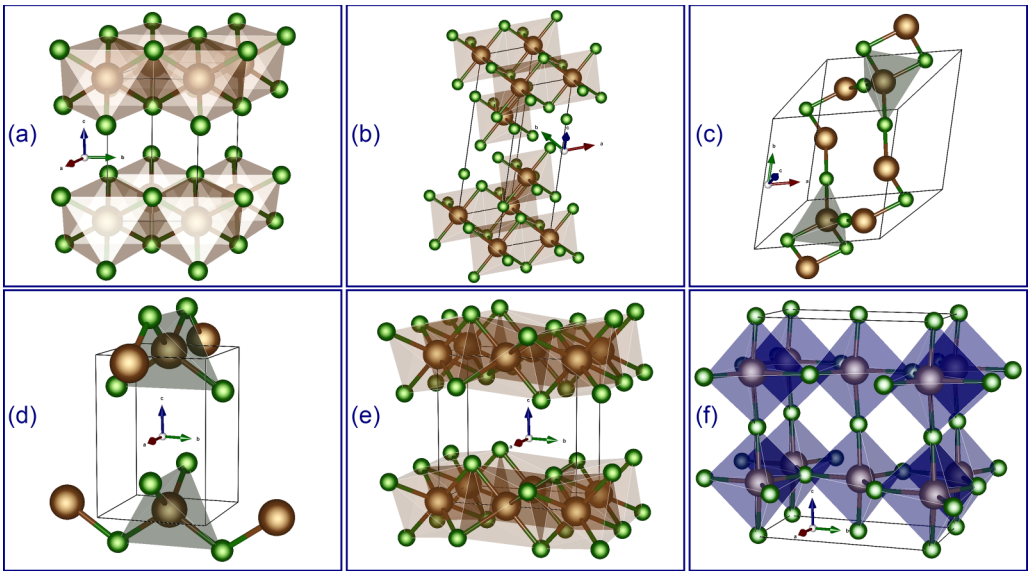

FIG. 7. Illustration of different (meta)stable $MgCl_2$ salt structures [64]. (a), (b), (e) Hexacoordinated. (f) Pentacoordinated. (c), (d) Tetracoordinated. The $MgCl_2$ salt structures in (a) and (b) have been found experimentally whereas structures in (c)–(f) correspond to numerically found metastable structures.

indicating the influence of the substrate and the necessity to accommodate lattice mismatch may induce local structural rearrangements at the interface.

Furthermore, we investigated the impact of dipole interactions by implementing linear dipole corrections to the potential and forces parallel to the direction of the third lattice vector within the simulation. This correction aimed to address errors introduced by periodic boundary conditions. However, the influence of dipole correction proved minimal, as simulations with and without dipole correction consistently converged onto similar stable structures. This observation held true for both the PBE and revised PBE from Hammer *et al.* [62], indicating the robustness of our findings across different computational methodologies.

Eventually the lattice mismatch and the resulting strain [63] at such interfaces will be healed by the formation of dislocations so that far away from the interface the two crystals have their native lattice constants. However, the computationally rather demanding inclusion of such dislocations is beyond the scope of the present paper. In any case, instead of the formation of thick $MgCl_2$ layers on Mg(0001) one rather expects eventually a complete conversion of the Mg metal to a $MgCl_2$ crystal upon continuous exposure of the Mg metal to chlorine.

To understand the different polyhedra present in this adsorption configuration, we examined the Mg-Cl coordinated distances in all $MgCl_2$ salt structures, which ranged from 2.35 Å for fourfold-coordinated configurations to a maximum of 2.67 Å for sixfold-coordinated configurations. The remarkable feature of the MgCl layer structure lies in the diverse coordination environments adopted by the top layer Mg atoms, with each being surrounded by three to six Cl atoms. By employing Voronoi polyhedra analysis, we quantified the local coordination environment of each Mg atom and determined the number of shared faces with neighboring atoms in the adsorption structure. To account for lattice mismatch effects, a slightly higher (8.6% compared to the maximum 2.67 Å Mg-Cl distance) coordination distance of 2.9 Å for Mg-Cl was adopted. Our analysis revealed that 22.2% of Mg atoms were threefold coordinated (with Mg-Cl bond distances between 2.43 and 2.69 Å), 33.3% were fourfold coordinated (with Mg-Cl bond distances between 2.3 and 2.45 Å), 22.2% were fivefold coordinated (with Mg-Cl bond distances between 2.35 and 2.67 Å), and 22.2% were sixfold coordinated (with Mg-Cl bond distances between 2.43 and 2.9 Å).

Indeed, the $\Theta = 2.0$ structure [Fig. 6(b)] does not correspond to a layer of any of the energetically possible $MgCl_2$ modifications [Figs. 7(a)–7(f)] due to the incompatibility arising from the lattice mismatch between the Mg(0001) substrate and the possible layer configurations. For a very similar reason, at the juncture where the metal slab meets the saltlike structures, the Mg atoms exhibit a tricoordinated arrangement, in contrast to the four to six coordinated Mg atoms characteristic of all known $MgCl_2$ salt structures. Nonetheless, as we move to elevated levels along the z axis, we do observe coordination environments that bear similarities to reported salt structures.

To assess the local coordination environments within the adsorption structures, we employed several robust goodness measures to compare polyhedral similarities for matching polyhedra of each top layer Mg atoms with reference salt structures. However, as none of them was sufficient to fully capture the complexities of structural similarity or dissimilarity between polyhedra, we leveraged local structure descriptors, specifically the radial pair distribution function (RDF), for the intuitive local perspective on the atomic arrangement around each atom [65]. The radial pair distribution function $g_{\alpha\beta}(r)$ quantifies the likelihood of finding a particle β at a distance r from a reference particle α, with α positioned at $r = 0$. Essentially, it creates a histogram of pairwise particle distances. In our case, involving two particle species, Mg and Cl, $g(r)$ yields three distinct partial functions:

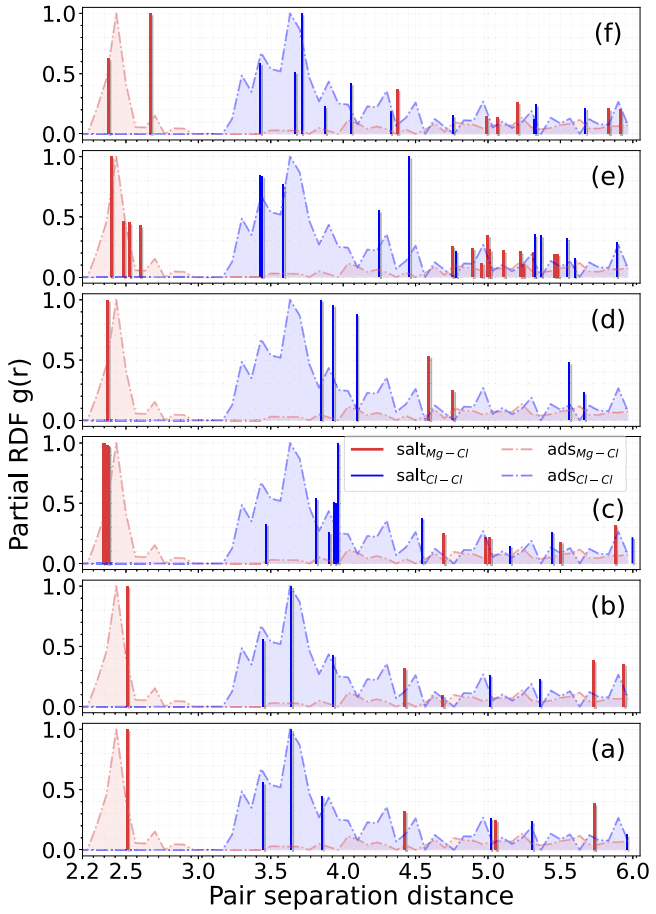

FIG. 8. Comparison of the radial distribution functions for Mg-Cl (red) and Cl-Cl (blue) distances. Dash-dotted lines: RDFs for the most stable Cl/Mg(0001) structure at a coverage of $\Theta_{HF_{2.0}}$, plotted in the background with a broadening. Bars: RDFs of the $MgCl_2$ salt structures depicted in Figs. 7(a)–7(f). (a) Experimental trigonal omega ($P3\bar{m}1$). (b) Experimental trigonal omega ($R\bar{3}m$). (c) Triclinic ($\bar{P}1$). (d) Tetragonal ($\bar{P}4m2$). (e) Orthorhombic ($Pmma$). (f) Orthorhombic ($Ama2$).

$g_{MgMg}(r)$, $g_{MgCl}(r)$, and $g_{ClCl}(r)$. We corroborate our findings by presenting a visual representation in Fig. 8, where we plot the normalized partial RDFs $g_{MgCl}(r)$ and $g_{ClCl}(r)$ of the adsorbate structure in the background, with normalized partial RDFs of experimental and theoretical $MgCl_2$ salt structures as foreground overlays. Here, "normalized" refers to scaling with respect to the maximum value of that particular partial RDF.

In Figs. 8(a) and 8(b), the juxtaposition showcases the seamless amalgamation of all foreground peaks within the background RDF. First of all, it is obvious that no RDF of one particular $MgCl_2$ bulk structure matches the RDF of the Cl adsorbate structure. However, all of the considered $MgCl_2$ bulk structures at least partially coincide with the surface salt structure. There is a particularly good agreement between the surface salt structure and the experimentally observed trigonal omega $P3\bar{m}1$ [Fig. 8(a)] and $R\bar{3}m$ [Fig. 8(b)] structures with respect to the Cl-Cl distances between 3.5 and 4.0 Å. Still, also the hypothetical structures in Figs. 8(c)–8(f) exhibit peaks that coincide with those of the surface salt structure. Apparently, due to the lattice and symmetry mismatch between the hexagonally close-packed Mg(0001) surface within a 3×3 surface unit cell and the $MgCl_2$ bulk structure, no single $MgCl_2$ bulk structure can be deposited onto Mg(0001) in a commensurate pattern. Yet, by combining structural motifs of various possible $MgCl_2$ bulk structures, a rather stable $MgCl_2$-surface salt structure can be created. Similar structures might also be formed on other Mg structures including stepped and nanostructured surfaces [66] which optimize the interaction strength between the Mg substrate and the chloride surface salt.

IV. CONCLUSIONS

In this theoretical paper, we have determined the energetically stable chlorine adsorbate structures on Mg(0001) for nominal chlorine coverages up to two monolayers. Such structures are relevant for the understanding of the conversion of the Mg anode in Cl-ion batteries upon discharge. Using a grand-canonical approach, we identified the thermodynamically stable Cl structures as a function of the applied electrode potential. Interestingly enough, it turns out that the layers with Cl atoms in the threefold hollow sites of Mg(0001) for a Cl coverage up to one monolayer are not thermodynamically stable. Instead, a three-dimensional surface salt structure with a nominal coverage of two chlorine monolayers identified by an adaptive random mutation hill climbing algorithm is the most stable structure. The comparison of the radial distribution function of this surface salt structure with those of various possible $MgCl_2$ bulk structures shows that the adsorbate structure is based on a combination of possible $MgCl_2$ bulk structural motifs.

The thermodynamically stable direct formation of a $MgCl_2$ surface salt structure on Mg(0001) suggests that the conversion of the Mg anode to a $MgCl_2$ configuration upon discharge of a Cl-ion battery is directly initiated upon the exposure of the Mg anode to chloride ions. The insights presented in our paper might therefore be beneficial in the optimization of future devices for electrochemical energy storage and conversion. Our paper can thus serve as a crucial stepping stone towards unlocking the full potential of halide adsorption in next-generation electrochemical technologies, offering promising prospects for sustainable and energy-efficient energy storage solutions.

ACKNOWLEDGMENTS

Financial support by the Dr. Barbara Mez-Starck Foundation and by the German Research Foundation under Project No. 390874152 (POLiS Cluster of Excellence, EXC 2154) is gratefully acknowledged. Computer time on the JUSTUS 2 cluster has been provided by the state of Baden-Württemberg through bwHPC and the German Research Foundation through Grant No. INST 40/575-1 FUGG. This work contributes to the research performed at the Center for Electrochemical Energy Storage Ulm-Karlsruhe (CELEST).

[1] O. M. Magnussen, Ordered anion adlayers on metal electrode surfaces, Chem. Rev. **102**, 679 (2002).

[2] F. Gossenberger, T. Roman, and A. Groß, Hydrogen and halide co-adsorption on Pt(111) in an electrochemical environment: a computational perspective, Electrochim. Acta **216**, 152 (2016).

[3] O. M. Magnussen and A. Groß, Toward an atomic-scale understanding of electrochemical interface structure and dynamics, J. Am. Chem. Soc. **141**, 4777 (2019).

[4] A. Groß, A. Eichler, J. Hafner, M. J. Mehl, and D. A. Papaconstantopoulos, Unified picture of the molecular adsorption process: O_2/Pt(111), Surf. Sci. **539**, L542 (2003).

[5] J. Yang, Y. Liu, Y. Zhang, G. Wang, X. Shi, H. Zhang, J. Li, P. Deng, and X. Tian, Recent advances and future perspectives of rechargeable chloride-based batteries, Nano Energy **110**, 108364 (2023).

[6] G. Karkera, M. A. Reddy, and M. Fichtner, Recent developments and future perspectives of anionic batteries, J. Power Sources **481**, 228877 (2021).

[7] X. Zhao, Z. Zhao-Karger, M. Fichtner, and X. Shen, Halide-based materials and chemistry for rechargeable batteries, Angew. Chem. Int. Ed. **59**, 5902 (2020).

[8] X. Zhao, Q. Li, Z. Zhao-Karger, P. Gao, K. Fink, X. Shen, and M. Fichtner, Magnesium anode for chloride ion batteries, ACS Appl. Mater. Interfaces **6**, 10997 (2014).

[9] Y. Tian, G. Zeng, A. Rutt, T. Shi, H. Kim, J. Wang, J. Koettgen, Y. Sun, B. Ouyang, T. Chen, Z. Lun, Z. Rong, K. Persson, and G. Ceder, Promises and challenges of next-generation "beyond Li-ion" batteries for electric vehicles and grid decarbonization, Chem. Rev. **121**, 1623 (2021).

[10] A. El Kharbachi, O. Zavorotynska, M. Latroche, F. Cuevas, V. Yartys, and M. Fichtner, Exploits, advances and challenges benefiting beyond Li-ion battery technologies, J. Alloys Compd. **817**, 153261 (2020).

[11] E. Bertel, K. Schwaha, and F. P. Netzer, Adsorption of bromine on Pt(111): Observation of an irreversible order-disorder transition, Surf. Sci. **83**, 439 (1979).

[12] W. Erley, Chlorine adsorption on the (111) faces of Pd and Pt, Surf. Sci. **94**, 281 (1980).

[13] A. Migani, C. Sousa, and F. Illas, Chemisorption of atomic chlorine on metal surfaces and the interpretation of the induced work function changes, Surf. Sci. **574**, 297 (2005).

[14] P. S. Bagus, C. Wöll, and A. Wieckowski, Dependence of surface properties on adsorbate-substrate distance: Work function changes and binding energy shifts for I/Pt(111), Surf. Sci. **603**, 273 (2009).

[15] T. Roman and A. Groß, Periodic density-functional calculations on work function change induced by adsorption of halogens on Cu(111), Phys. Rev. Lett. **110**, 156804 (2013).

[16] F. Gossenberger, T. Roman, K. Forster-Tonigold, and A. Groß, Change of the work function of platinum electrodes induced by halide adsorption, Beilstein J. Nanotechnol. **5**, 152 (2014).

[17] T. Roman, F. Gossenberger, K. Forster-Tonigold, and A. Groß, Halide adsorption on close-packed metal electrodes, Phys. Chem. Chem. Phys. **16**, 13630 (2014).

[18] P. Zhou, C. Zhou, and H. Gong, Chlorine adsorption on Mg, Ca, and MgCa surfaces, Mater. Sci. Eng. C **33**, 3826 (2013).

[19] Y.-H. Duan, Adsorption of fluorine and chlorine on Mg(0001) surface: A density functional theory investigation, Trans. Nonferrous Met. Soc. China **24**, 1844 (2014).

[20] Z. Luo, H. Zhu, T. Ying, D. Li, and X. Zeng, First principles calculations on the influence of solute elements and chlorine adsorption on the anodic corrosion behavior of Mg(0001) surface, Surf. Sci. **672–673**, 68 (2018).

[21] D. J. Siegel, L. G. Hector, and J. B. Adams, Adhesion, atomic structure, and bonding at the $Al(111)/\alpha - Al_2O_3(0001)$ interface: A first principles study, Phys. Rev. B **65**, 085415 (2002).

[22] K. Leung, First principles, explicit interface studies of oxygen vacancy and chloride in alumina films for corrosion applications, J. Electrochem. Soc. **168**, 031511 (2021).

[23] Q. Campbell, Voltage-dependent first-principles simulation of insertion of chloride ions into Al/Al_2O_3 interfaces using the quantum continuum approximation, J. Electrochem. Soc. **170**, 031506 (2023).

[24] T. Li, D. Perea, D. Schreiber, M. G. Wirth, G. J. Orren, and G. Frankel, Cryo-based structural characterization and growth model of salt film on metal, Corros. Sci. **174**, 108812 (2020).

[25] C. D. Taylor, S. Li, and A. J. Samin, Oxidation versus salt-film formation: Competitive adsorption on a series of metals from first-principles, Electrochim. Acta **269**, 93 (2018).

[26] K. W. Leong, W. Pan, Y. Wang, S. Luo, X. Zhao, and D. Y. C. Leung, Reversibility of a high-voltage, Cl-regulated, aqueous Mg metal battery enabled by a water-in-salt electrolyte, ACS Energy Lett. **7**, 2657 (2022).

[27] M. Salama, I. Shterenberg, L. J.W. Shimon, K. Keinan-Adamsky, M. Afri, Y. Gofer, and D. Aurbach, Structural analysis of magnesium chloride complexes in dimethoxyethane solutions in the context of Mg batteries research, J. Phys. Chem. C **121**, 24909 (2017).

[28] M. Todorova, E. Lundgren, V. Blum, A. Mikkelsen, S. Gray, J. Gustafson, M. Borg, J. Rogal, K. Reuter, J. Andersen, and M. Scheffler, The $Pd(100) - (5 \times 5)R27^\circ - O$ surface oxide revisited, Surf. Sci. **541**, 101 (2003).

[29] E. Lundgren, A. Mikkelsen, J. N. Andersen, G. Kresse, M. Schmid, and P. Varga, Surface oxides on close-packed surfaces of late transition metals, J. Phys.: Condens. Matter **18**, R481 (2006).

[30] X. Lin, F. Gossenberger, and A. Groß, Ionic adsorbate structures on metal electrodes calculated from first-principles, Ind. Eng. Chem. Res. **55**, 11107 (2016).

[31] X. Lin, X. Tian, L. Song, M. Hua, and A. Groß, Restructuring of lead electrodes upon adsorption of NO_3^- anions studied from first-principles and its relevance for the operation of lead quantum switches, J. Phys. Chem. C **125**, 17962 (2021).

[32] F. Xie, R. Maul, C. Obermair, W. Wenzel, G. Schön, and T. Schimmel, Multilevel atomic-scale transistors based on metallic quantum point contacts, Adv. Mater. **22**, 2033 (2010).

[33] F.-Q. Xie, X.-H. Lin, A. Gross, F. Evers, F. Pauly, and T. Schimmel, Multiplicity of atomic reconfigurations in an electrochemical Pb single-atom transistor, Phys. Rev. B **95**, 195415 (2017).

[34] M. Jäckle, K. Helmbrecht, M. Smits, D. Stottmeister, and A. Groß, Self-diffusion barriers: Possible descriptors for dendrite growth in batteries? Energy Environ. Sci. **11**, 3400 (2018).

[35] K. Reuter and M. Scheffler, Composition, structure, and stability of $RuO_2(110)$ as a function of oxygen pressure, Phys. Rev. B **65**, 035406 (2001).

[36] A. A. Peterson, F. Abild-Pedersen, F. Studt, J. Rossmeisl, and J. K. Nørskov, How copper catalyzes the electroreduction of carbon dioxide into hydrocarbon fuels, Energy Environ. Sci. **3**, 1311 (2010).

[37] A. Groß, Grand-canonical approaches to understand structures and processes at electrochemical interfaces from an atomistic perspective, Curr. Opin. Electrochem. **27**, 100684 (2021).

[38] A. Groß, Reversible vs standard hydrogen electrode scale in interfacial electrochemistry from a theoretician's atomistic point of view, J. Phys. Chem. C **126**, 11439 (2022).

[39] G. Kresse and J. Furthmüller, Efficient iterative schemes for ab initio total-energy calculations using a plane-wave basis set, Phys. Rev. B **54**, 11169 (1996).

[40] G. Kresse and J. Furthmüller, Efficiency of *ab-initio* total energy calculations for metals and semiconductors using a plane-wave basis set, Comput. Mater. Sci. **6**, 15 (1996).

[41] H. Euchner and A. Groß, Atomistic modeling of Li- and post-Li-ion batteries, Phys. Rev. Mater. **6**, 040302 (2022).

[42] J. P. Perdew, K. Burke, and M. Ernzerhof, Generalized gradient approximation made simple, Phys. Rev. Lett. **77**, 3865 (1996).

[43] M. Jäckle and A. Groß, Influence of electric fields on metal self-diffusion barriers and its consequences on dendrite growth in batteries, J. Chem. Phys. **151**, 234707 (2019).

[44] P. E. Blöchl, Projector augmented-wave method, Phys. Rev. B **50**, 17953 (1994).

[45] G. Kresse and D. Joubert, From ultrasoft pseudopotentials to the projector augmented-wave method, Phys. Rev. B **59**, 1758 (1999).

[46] C. Kittel, *Introduction to Solid State Physics* (Wiley, New York, 2005).

[47] G. Walker and M. Marezio, Lattice parameters and zone overlap in solid solutions of lead in magnesium, Acta Metall. **7**, 769 (1959).

[48] E. R. Jette and F. Foote, Precision determination of lattice constants, J. Chem. Phys. **3**, 605 (1935).

[49] H. A. Hansen, I. C. Man, F. Studt, F. Abild-Pedersen, T. Bligaard, and J. Rossmeisl, Electrochemical chlorine evolution at rutile oxide (110) surfaces, Phys. Chem. Chem. Phys. **12**, 283 (2010).

[50] F. Gossenberger, T. Roman, and A. Groß, Equilibrium coverage of halides on metal electrodes, Surf. Sci. **631**, 17 (2015).

[51] M. Lischka, C. Mosch, and A. Groß, Tuning catalytic properties of bimetallic surfaces: Oxygen adsorption on pseudomorphic Pt/Ru overlayers, Electrochim. Acta **52**, 2219 (2007).

[52] A. Groß, *Theoretical Surface Science: A Microscopic Perspective*, 2nd ed. (Springer-Verlag, Berlin, 2009).

[53] J. L. Da Silva, C. Stampfl, and M. Scheffler, Converged properties of clean metal surfaces by all-electron first-principles calculations, Surf. Sci. **600**, 703 (2006).

[54] P. Sprunger, K. Pohl, H. Davis, and E. Plummer, Multilayer relaxation of the Mg(0001) surface, Surf. Sci. **297**, L48 (1993).

[55] Ismail, P. Hofmann, A. P. Baddorf, and E. W. Plummer, Thermal expansion at a metal surface: A study of Mg(0001) and Be(10$\bar{1}$0), Phys. Rev. B **66**, 245414 (2002).

[56] Y. Li, P. Zhang, B. Sun, Y. Yang, and Y. Wei, Atomic hydrogen adsorption and incipient hydrogenation of the Mg(0001) surface: A density-functional theory study, J. Chem. Phys. **131**, 034706 (2009).

[57] K. Sarkar and S. P. Bhattacharyya, Single string based global optimizer for geometry optimization in strongly coupled finite clusters: An adaptive mutation-driven strategy, J. Chem. Phys. **139**, 074106 (2013).

[58] K. Sarkar and S. P. Bhattacharyya, *Soft Computing in Chemical and Physical Sciences: A Shift in Computing Paradigm* (CRC, Boca Raton, FL, 2017).

[59] K. Sarkar, N. Holzwarth, and R. Wentzcovitch, Epaw-1.0 code for evolutionary optimization of paw datasets especially for high-pressure applications, Comput. Phys. Commun. **233**, 110 (2018).

[60] I. W. Bassi, F. Polato, M. Calcaterra, and J. C. J. Bart, A new layer structure of $MgCl_2$ with hexagonal close packing of the chlorine atoms, Z. Kristallogr. **159**, 297 (1982).

[61] D. Partin and M. O'Keeffe, The structures and crystal chemistry of magnesium chloride and cadmium chloride, J. Solid State Chem. **95**, 176 (1991).

[62] B. Hammer, L. B. Hansen, and J. K. Nørskov, Improved adsorption energetics within density-functional theory using revised Perdew-Burke-Ernzerhof functionals, Phys. Rev. B **59**, 7413 (1999).

[63] A. Groß, Tailoring the reactivity of bimetallic overlayer and surface alloy systems, J. Phys.: Condens. Matter **21**, 084205 (2009).

[64] A. Jain, S. P. Ong, G. Hautier, W. Chen, W. D. Richards, S. Dacek, S. Cholia, D. Gunter, D. Skinner, G. Ceder, and K. A. Persson, Commentary: The Materials Project: A materials genome approach to accelerating materials innovation, APL Mater. **1**, 011002 (2013).

[65] M. W. Terban and S. J. L. Billinge, Structural analysis of molecular materials using the pair distribution function, Chem. Rev. **122**, 1208 (2022).

[66] A. Groß, Adsorption at nanostructured surfaces from first principles, J. Comput. Theor. Nanosci. **5**, 894 (2008).